High-Temporal-Resolution Capabilities of the National Weather Radar Testbed Phased-Array Radar

PAMELA L. HEINSELMAN

NOAA/OAR/National Severe Storms Laboratory, Norman, Oklahoma

SEBASTIÁN M. TORRES

*Cooperative Institute for Mesoscale Meteorological Studies, University of Oklahoma, and NOAA/OAR/National
Severe Storms Laboratory, Norman, Oklahoma*

ABSTRACT

Since 2007 the advancement of the National Weather Radar Testbed Phased-Array Radar (NWRT PAR) hardware and software capabilities has been supporting the implementation of high-temporal-resolution (~1 min) sampling. To achieve the increase in computational power and data archiving needs required for high-temporal-resolution sampling, the signal processor was upgraded to a scalable, Linux-based cluster with a distributed computing architecture. The development of electronic adaptive scanning, which can reduce update times by focusing data collection on significant weather, became possible through functionality added to the radar control interface and real-time controller. Signal processing techniques were implemented to address data quality issues, such as artifact removal and range-and-velocity ambiguity mitigation, absent from the NWRT PAR at its installation. The hardware and software advancements described above have made possible the development of conventional and electronic scanning capabilities that achieve high-temporal-resolution sampling. Those scanning capabilities are sector- and elevation-prioritized scanning, beam multiplexing, and electronic adaptive scanning. Each of these capabilities and related sampling trade-offs are explained and demonstrated through short case studies.

1. Introduction

The need for high-temporal-resolution data (~1 min) to improve the depiction, understanding, and warning of hazardous weather phenomena has been understood for some time (e.g., Miller and Kropfli 1980; Carbone et al. 1985) and continues to drive radar research and demonstration initiatives (e.g., Wilson et al. 1984; Lin et al. 1986; Qiu and Xu 1996; Wurman 2002; Bluestein and Wakimoto 2003; Zrnić et al. 2007; Heinselman et al. 2008; Bluestein et al. 2010; Kumjian et al. 2010; Yussouf and Stensrud 2010). For example, in 2010 the second Verification of the Origin of Rotation in Tornadoes Experiment (VORTEX2) used short-wavelength (3 and 5 cm) mobile radars to collect rapid-scan data to improve our understanding of tornadogenesis (information online at http://www.vortex2.org). In another research initiative, the Center for Collaborative Adapting Sensing of the Atmosphere (CASA) has been investigating the use of distributed collaborative adaptive sensing to produce rapid-scan, low-altitude sampling of storms with a network of four low-power, short-wavelength (3 cm), mechanically scanning radars (Junyent et al. 2010; McLaughlin et al. 2009).

Since May 2004, scientists at the National Severe Storms Laboratory (NSSL) have been exploring the high-temporal-resolution weather scanning capabilities of an S-band (9.38 cm), agile-beam, phased-array radar system. Located in Norman, Oklahoma, this system is referred to as the National Weather Radar Testbed Phased-Array Radar (NWRT PAR). The system is part of the broader multifunction phased-array radar (MPAR) initiative that is investigating the use of a single radar system to perform both weather and aircraft surveillance functions (Weber et al. 2007; National Academies 2008). Interested readers may refer to Zrnić et al. (2007) for a detailed, technical description of the NWRT PAR.

Corresponding author address: Dr. Pamela L. Heinselman, 120 David L. Boren Blvd., Norman, OK 73072.
E-mail: pam.heinselman@noaa.gov

Briefly, the NWRT PAR exploits a passive, 4352-element phased-array antenna to provide stationary, two-dimensional electronic scanning of weather echoes within a given 90° azimuthal sector. The antenna is mounted on a turntable to allow focused data collection in the direction of greatest meteorological interest. The two-way, 6-dB antenna beamwidth is 1.6° at boresight (i.e., perpendicular to the array plane) and gradually increases to 2.3° at ±45° from boresight. The peak transmitted power is 750 kW and the range resolution provided by this system is 240 m. In some aspects, such as beamwidth and sensitivity, the NWRT PAR is inferior compared to operational radars such as the Weather Surveillance Radar-1988 Doppler (WSR-88D). However, the purpose of this system is not to achieve operational-like performance or to serve as a prototype for the MPAR, but to demonstrate the operational utility of some of the unique capabilities offered by PAR technology that may eventually drive the design of future operational weather radars.

A key capability of PAR technology is high-temporal-resolution sampling that can be achieved through many methods. As illustrated in Heinselman et al. (2008), data collection with the NWRT PAR over a 90° sector, rather than over a typical 360° sector, produces faster updates than would otherwise be possible. Because a future operational system would likely have a multipanel design that samples a full 360° sector, the NWRT PAR demonstrates this design-driven rapid-scan capability. Moreover, the NWRT PAR's electronic beam steering allows the development of unique sampling techniques like beam multiplexing (Yu et al. 2007) and weather-focused electronic adaptive scanning that can further reduce sampling time.

The purpose of this paper is fourfold: 1) to document the advancement of NWRT PAR hardware and software capabilities that support high-temporal-resolution sampling of weather, 2) to provide an analysis of the trade-offs involved in the design of rapid-scanning strategies, 3) to describe the weather-focused adaptive scanning technique currently implemented on the NWRT PAR, and 4) to illustrate examples of high-temporal sampling employed by this unique radar system. Although most of the trade-off analysis can be extended to other radar systems, the focus of this work is on the NWRT PAR.

2. NWRT PAR upgrades

Significant hardware and software upgrades have been and are needed to support the NWRT mission as a demonstrator system for the MPAR concept. Since 2007, scientists and engineers at NSSL have been improving the functionality and capabilities of the NWRT PAR. These upgrades are summarized next.

a. Hardware upgrades

Soon after deployment of the NWRT PAR, it became apparent that proposed increasing needs for computational power and archiving of time series and meteorological data were unsustainable with the original signal processing hardware. Accordingly, the radar signal processor was upgraded from a discontinued, proprietary cluster of multiprocessor boards manufactured by SKY Computers, Inc., to a Linux-based cluster of multiple dual-processor, dual-core nodes that communicate via a high-speed interconnect (Forsyth et al. 2007). The architecture of the new signal processor is based on distributed computing. That is, all nodes in the cluster work toward the common goal of real-time radar signal processing. The system is designed to optimally utilize the nodes (i.e., computational resources). Specifically, a load-balancing mechanism, in which nodes compete to read and process sets of radar data, tailors the data distribution to each node at a rate according to their capabilities. In this way, the system's scalability is facilitated by allowing a hybrid mixture of nodes in the cluster. The signal processor cluster is complemented by a 12-TB redundant storage system [Redundant Array of Independent Disks (RAID)] that supports simultaneous, continuous recording of time series and meteorological quantities (i.e., reflectivity, Doppler velocity, and spectrum width) for about 175 h.

b. Software upgrades

The deployment of the new signal processing hardware marked the beginning of a series of software upgrades. Using a path of continuous upgrades with an average of two releases every year, we have been gradually incorporating new and improved functionality to the NWRT PAR. The need for software and signal processing improvements is twofold. On one hand, it is desirable that the NWRT PAR produces operational-like data with quality comparable to that of the WSR-88D. High data quality leads to better data interpretation and is conducive to the development of automatic algorithms. On the other hand, improvements are needed to demonstrate new capabilities, some of which are applicable to conventional and phased-array radars, and some that are unique or better suited to PAR technology. For example, the use of adaptive scanning strategies to perform focused observations of the atmosphere is not unique to PAR (e.g., Chrisman 2009), but update times can be greatly reduced by using PAR's electronic beam-steering capabilities to scan individual storms of interest as opposed to
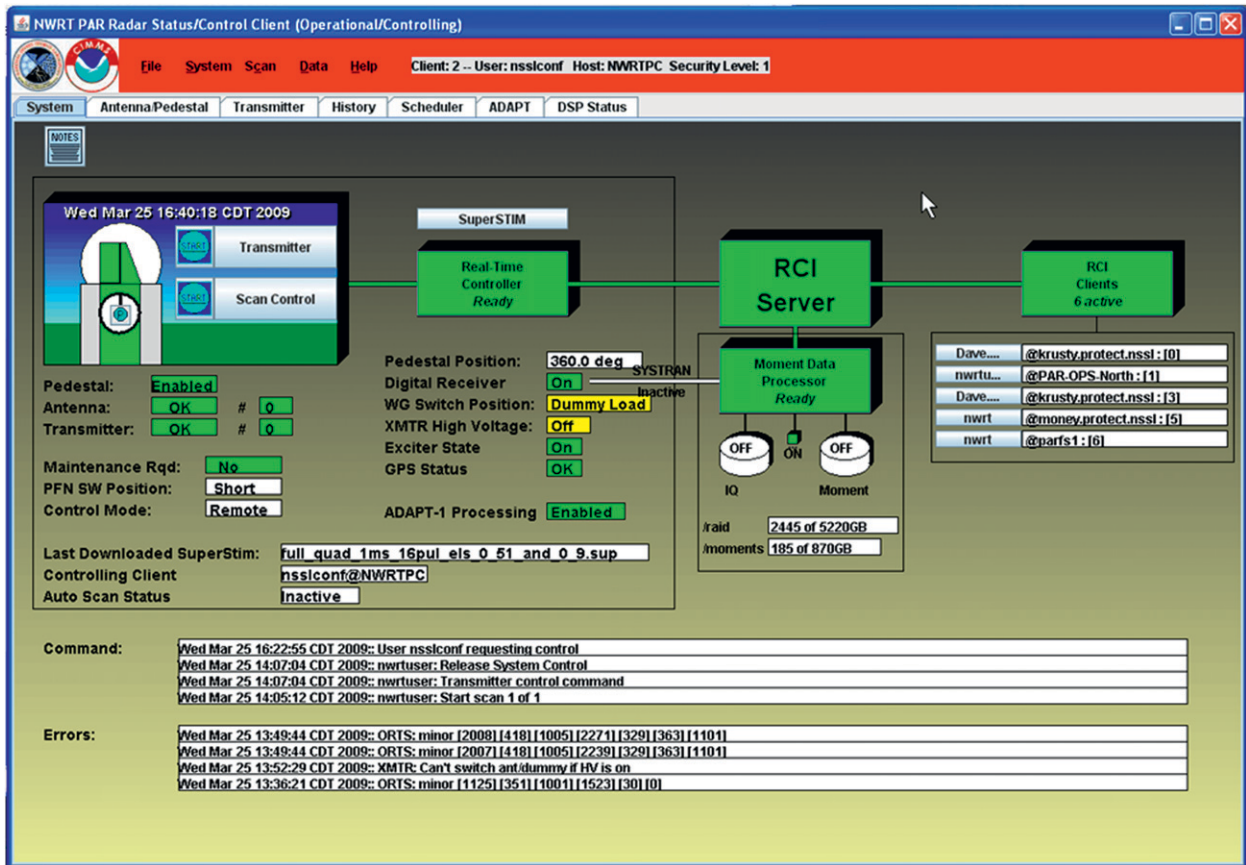
FIG. 1. The RCI for the NWRT PAR. From a user perspective, all radar functions on the NWRT PAR are controlled and monitored by the RCI.

having to overcome the mechanical inertia inherent to reflector antennas.

1) INFRASTRUCTURE UPGRADES

The software infrastructure was drastically revamped to support the implementation of new functionality in three major areas: the distributed computing environment, the user interface, and the real-time controller. The message-based, signal processing-cluster infrastructure was modeled after the Next Generation Weather Radar (NEXRAD) Open Radar Product Generation design (Jain et al. 1997). This type of design allows for the seamless integration of nodes in the cluster, and provides the required computational power to implement traditional as well as advanced signal processing techniques.

The radar control interface (RCI) is a Java-based graphical user interface that provides radar control and status monitoring (Fig. 1). The standard RCI functionality allows radar operators to complete tasks such as rotating the antenna pedestal, selecting scanning strategies, turning the radar on and off, and controlling data archiving. In addition to these and many other basic control functions, the RCI has been significantly improved to demonstrate new capabilities (Priegnitz et al. 2009). For example, the system allows radar operators to dynamically select a sequence of scanning strategies and modify any of their parameters in real time. The dynamic selection of scanning characteristics is being evaluated as a manual capability, but will eventually lead to the design of new, advanced adaptive scanning algorithms. At the same time, the RCI provides a means to assess the performance of existing adaptive scanning algorithms in real time by providing a graphical display of active and inactive beam positions (Fig. 2; the current adaptive algorithm is described in section 4).

The real-time controller (RTC) is the nexus with the rest of the radar hardware. The RTC provides control of antenna positioning, the transmitter, and the receiver. RTC updates support multifunction capabilities by tagging received signals for function-specific processing. Also, the RTC receives commands from the signal processor to perform adaptive scanning by turning on and off selected beam positions. In the autumn of 2011, we plan to support schedule-based scanning by
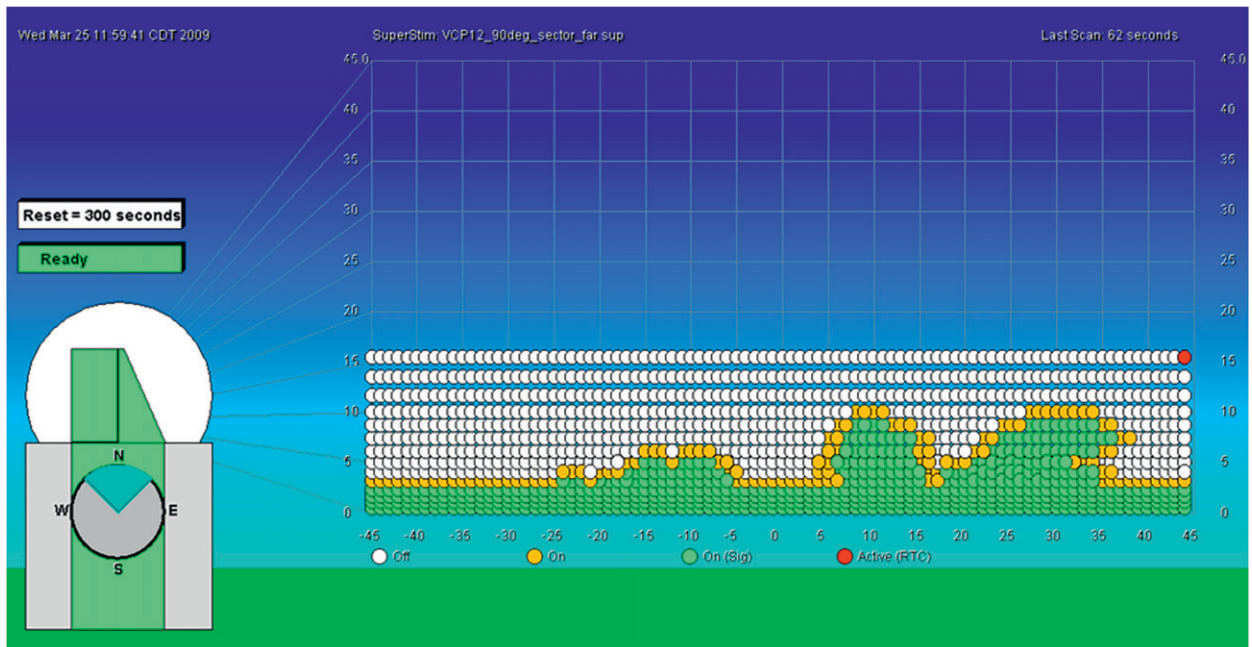
FIG. 2. Depiction of ADAPTS's real-time performance at the NWRT PAR user interface. Beam positions on an azimuth-by-elevation plane are color coded as follows: white beam positions are inactive, green beam positions are active based on elevation and coverage criteria, and orange beam positions are active based on the neighborhood criterion.

removing the scan-processing functionality from the RTC and providing scan information directly from the signal processor. This will allow better real-time control of scanning strategies driven by an automatic scheduling algorithm and will therefore enable more advanced adaptive scanning schemes.

Improvements to the archiving function were also needed to support the recording and playback capabilities necessary in a research and development environment. The playback function is routinely used to evaluate the performance of signal processing techniques and fine-tune algorithm parameters. Also, because the system is in constant evolution, playback is often used to reprocess time series data with the latest capabilities and obtain the best possible quality of the meteorological data. Moreover, the recording and playback functions are key components of the yearly spring experiments conducted at the NWRT (Heinselman et al. 2009) as they allow participants to work "on demand" with a diverse set of weather situations from our archive.

2) SIGNAL PROCESSING UPGRADES

Signal processing enhancements are a fundamental part of the NWRT PAR upgrades with both traditional and advanced signal processing techniques being implemented and tested in a pseudo-operational environment. Traditional signal processing techniques are exploited to achieve performance similar to that of WSR-88Ds. This

facilitates data analyses and comparisons with existing operational data. Additionally, we are able to transition our latest research into the NWRT PAR in the form of advanced signal processing techniques.

To support the evolutionary nature of the signal processing capabilities on the NWRT PAR, we designed a flexible and expandable architecture based on "processing modes." Each processing mode ingests time series data (i.e., in-phase and quadrature samples) and produces spectral moment data (i.e., reflectivity, Doppler velocity, and spectrum width) in fundamentally different ways. To date, the system supports five processing modes: three modes operate in the time domain and two in the frequency domain. Processing modes are data-driven signal processing pipelines (i.e., sequences of processing blocks) that can be controlled with a set of "processing options." These are user-defined, editable control flags and parameters for the processing blocks that compose a processing mode.

Signal processing techniques address needs in four major areas: calibration, artifact removal, range-and-velocity ambiguity mitigation, and data accuracy. As of December 2009, the system runs a few automatic calibration routines such as noise power and direct-current (DC) bias measurements. Reflectivity calibration is performed offline at boresight and adjusted in real time for off-boresight beam positions (Zhang et al. 2008). Time series data are filtered to mitigate contamination from

radio-frequency interference, strong point targets such as airplanes, and stationary returns from the ground such as buildings and trees. Ground clutter detection and filtering is done automatically in real time and the filter's suppression is adjusted based on the strength of the contamination (Warde and Torres 2009). To mitigate range and velocity ambiguities (Doviak and Zrnić 2006), the signal processor can ingest multiple-pulse-repetition-time (PRT) data such as "batch" or staggered PRT (Torres et al. 2004). In addition, the accuracy of meteorological data can be improved by using range oversampling techniques (Torres and Zrnić 2003) or beam multiplexing (Yu et al. 2007).

3. Design of scanning strategies for the NWRT PAR

Pulsed weather radars continuously sample the atmosphere in three dimensions, and scanning strategies are used to control how this sampling occurs. The effective design of scanning strategies involves tailoring spatial sampling and data acquisition parameters for a specific need or particular meteorological situation. Herein, we discuss the considerations and trade-offs involved in the design of scanning strategies. Although most of this analysis can be extended to other radar systems, the focus is on the NWRT PAR.

Spatial sampling occurs on a volumetric grid defined on spherical coordinates: range, azimuth, and elevation. The grid spacing in range is controlled by the sampling period of echoes at the radar receiver, and grid spacing is usually chosen to match the depth of the radar's resolution volume to produce independent estimates of meteorological variables along the beam (Doviak and Zrnić 2006). However, oversampling in range can be used to reduce the uncertainty of weather data without increasing update times (Torres and Zrnić 2003). In the NWRT PAR, typical range spacing is 240 m, though the system can oversample by factors of 4, 8, or 16. The main trade-off associated with range oversampling is related to the data throughput and computational complexity that are required with finer sampling. On the other hand, sampling in azimuth and elevation determines the number of beam positions in the scanning strategy and leads to more fundamental trade-offs discussed next.

The scan update time (UT) is defined as the time to complete the execution of a scanning strategy and can be computed as

$$UT = \sum_{i=1}^{BP} DT_i, \qquad (1)$$

where BP is the number of beam positions in the scanning strategy and DT_i is the dwell time corresponding to the ith beam position. This equation shows that the scan update time is directly proportional to the number of antenna beam positions in the scanning strategy, which, in turn, is dictated by the sampling in azimuth and elevation.

The azimuthal sampling is usually set to match the antenna beamwidth so that complete coverage can be obtained with the minimum number of beam positions. Nevertheless, oversampling (i.e., overlapped beams) can be used advantageously once again, in this case, to improve observations of small-scale features at long ranges such as with super-resolution on the NEXRAD network (Brown et al. 2002; Torres and Curtis 2007). Because the NWRT PAR's antenna is stationary during data collection, the beam-smearing effect from continuously rotating antennas is absent. The azimuthal beam resolution with electronic beam steering is solely determined by the antenna beam pattern. The combination of finer azimuthal sampling and the absence of beam smearing can provide improved observations of reflectivity and velocity magnitude, and as a result enhanced depictions of storm structure. The number of beam positions in the azimuth is determined by the extent of coverage and the desired sampling resolution. In the NWRT PAR, the size of the azimuthal sector is limited by electronic beam steering to ±45° relative to the boresight.

The required vertical resolution and extent of coverage determines the sampling in elevation. Usually finer vertical resolution is desired closer to the ground, but due to the inherent coordinate system or the radar sampling grid, vertical resolution varies as a function of range. Storm tops and their range may be used to determine the highest elevation angle of beam positions needed to sample an entire storm. As such, nearby storms would require larger elevation spans and vice versa. In the NWRT PAR, elevation angles can range from 0.5° to 60°.

In addition to being dependent on the number of beam positions, the scan update time is directly proportional to the dwell times defined by the scanning strategy. The dwell time is the time spent at a given beam position; it depends on the waveform, PRT(s), and desired number of samples (pulses). In the NWRT PAR, available waveforms are uniform PRT, batch PRT, staggered PRT, and beam multiplexing (BMX). The PRT controls the maximum unambiguous range and velocity, but different waveforms, such as staggered PRT, can be used to mitigate ambiguities (e.g., Torres et al. 2004). In the NWRT PAR, the PRT can range from 0.8 to 3.2 ms. Dwell times can be reduced by reducing the PRT(s) or the number of samples. Reducing the PRT may increase the likelihood of overlaid echoes, and reducing the number of samples can affect the performance of some signal

processing techniques, such as ground clutter filtering, which require a minimum number of samples for adequate suppression. In general, short dwell times result in reduced data quality. Nevertheless, there are techniques that can be used to reduce dwell times without sacrificing data quality. For example, range oversampling techniques (Torres and Zrnić 2003) use faster sampling rates at the radar receiver so that more samples are acquired in range without increasing the dwell times; range samples collected in this way can be decorrelated and used to reduce the variance of estimates via averaging. Conversely, dwell times can be increased without increasing the update time. Beam multiplexing (Yu et al. 2007) exploits beam agility to ''multitask'' by interlacing the sampling of multiple beam positions, which leads to longer dwell times without increasing the overall scan update time.

In summary, the scan update time can be reduced by reducing either the number of beam positions or dwell times. That is, achieving faster data updates leads to a trade-off between spatial resolution and data quality.

Examples of trade-offs

The concept of designing custom scanning strategies is not unique to PAR-based systems. For instance, the NEXRAD network uses precipitation and clear-air scanning strategies with different trade-offs (NOAA 2006, 5-1–5-8); three examples follow. Precipitation volume coverage pattern (VCP) 21 comprises nine elevation tilts (0.5°–19.5°) and employs long dwell times resulting in a 6-min scan update. This scanning strategy trades improved data quality for longer update times and coarser vertical sampling. Precipitation VCP 12 comprises 14 tilts (0.5°–19.5°) and employs short dwell times resulting in a ~4-min scan update. This strategy trades faster updates and denser vertical sampling at the lower tilts for reduced data quality (higher variance of estimates). Clear-air VCP 31 comprises five tilts (0.5°–4.5°) and employs long dwell times with a 10-min scan update. This strategy trades improved detection and better data quality for longer update times and limited vertical sampling.

Similarly, for NWRT PAR we have adopted phenomenon-specific scanning strategies. These achieve the best trade-offs for a particular situation. Improved spatial resolution is achieved with scanning strategies employing higher-resolution vertical and/or azimuthal sampling. Unique to the PAR is that the inherent beam broadening that occurs as the beam is electronically steered away from boresight can be exploited to reduce the number of beam positions and obtain faster updates (e.g., to completely cover a 90° sector, only 55 nonoverlapping radials are needed).

For improved temporal resolution there are different options. BMX can be exploited to produce data with lower variance and faster updates. Yu et al. (2007) report it is possible to reduce the scan time by a factor of 2–4 without an increase in the variance of estimates at high signal-to-noise ratios. The trade-off is one of data quality since effective ground clutter filters that are compatible with the nonuniform signal sampling of BMX do not exist. This trade-off may be acceptable when weather is located outside of the area contaminated by ground clutter. As another option for improved temporal resolution, more frequent updates for the lowest tilt are achievable by adding a low-elevation scan halfway through the scanning strategy. This results in good data quality, but faster updates are only realized at the lowest tilt and this leads to slightly slower updates elsewhere. Through elevation-prioritized scanning, different updates at different levels can be achieved. In general, the fastest updates occur at the lowest tilts for the best temporal resolution closer to the ground. Intermediate tilts are updated less frequently, enough to detect new storm developments with short latency. Finally, the upper tilts get the slowest updates. Another way to improve the temporal resolution of the NWRT PAR without loss in data quality is to scan less than the full 90°. However, new developments outside the reduced sector are likely to be missed. An optimum compromise to produce good quality data with faster updates is to employ adaptive scanning techniques that automatically focus data collection on smaller areas of interest at the same time that periodic surveillance is performed to capture new storm developments. This automatic algorithm is described in the next section. Though many of these methods for reducing update time either have been (e.g., Vasiloff et al. 1987; Biggerstaff et al. 2005; Chrisman 2009; McLaughlin et al. 2009) or can be implemented on radars with mechanically scanning antennas, the resulting pedestal inertia and increased wear and tear associated with faster rotation rates make them better suited to stationary, electronically steered antennas.

4. ADAPTS: Adaptive Digital Signal Processing Algorithm for PAR Timely Scans

ADAPTS is a proof-of-concept implementation of spatially targeted adaptive scanning for the electronically steered NWRT PAR. Preliminary evaluations of ADAPTS have shown that the performance improvement with weather-focused adaptive scanning can be significant compared to conventional scanning strategies, especially when observing isolated storms as illustrated in section 5. ADAPTS works by turning ''on'' or ''off''

individual beam positions within a scanning strategy based on three criteria. If one or more criteria are met, the beam position is declared active. Otherwise, the beam position is declared inactive. Active beam position settings are applied and become valid on the next execution of a given scanning strategy. Additionally, ADAPTS periodically completes a complete volumetric surveillance scan, which is used to redetermine where weather echoes are located. A user-defined parameter controls the time between full surveillance scans (by default this is set at 5 min). Following a surveillance scan, data collection continues only on the active beam positions.

A beam position becomes active if one or more of the following criteria are met: 1) reflectivities along the beam meet continuity, coverage, and significance conditions; 2) the elevation angle is below a predefined level; or 3) a "neighboring" beam position is active based on the first or second criteria. The first criterion uses continuity, coverage, and significance conditions to make a quantitative determination of the amount of significant weather returns at each beam position. Within this context, a beam position is active if it contains (a) a certain number of consecutive range gates (by default four) with reflectivities exceeding a threshold (by default 10 dBZ) and (b) a total areal coverage (by default 1 km^2) with reflectivities exceeding the same threshold (that areal coverage is computed as the product of the range spacing and the gate width, which depends on the distance from the radar and the two-way, 6-dB antenna beamwidth). The second criterion provides data collection at all beam positions for the lowest elevation angles to monitor low-altitude developments. A user-defined elevation threshold (2.5° by default) controls the lowest elevation angle where ADAPTS may begin to deactivate beam positions. The third criterion uses neighboring beam positions to expand the data collection footprint to allow for continuous adaptation in response to storm advection and growth. Nevertheless, new developments at midlevels may not be immediately sensed, and therefore additions to the list of active beam positions may be delayed until the next full surveillance volume scan. Neighboring beam positions are defined as those immediately above and below in elevation and two on either side in azimuth of an active beam position (i.e., there are a total of six neighbors for each beam position, unless the scanning domain boundaries are approached). If no beam positions are defined active above the user-defined elevation threshold (criterion 2), ADAPTS will activate all beam positions at the tilt directly above the elevation threshold.

In its early implementation, ADAPTS only worked with scanning strategies that had a specific structure. ADAPTS assumed that there was only one plan position indicator (PPI) scanning strategy that repeated continuously. The algorithm also expected that all tilts were in ascending elevation order, and all used the same beam position azimuths with a minimum azimuthal spacing of 0.5° (i.e., the maximum number of beam positions for all elevations is 180). These limitations were removed with the next upgrade cycle during spring of 2010.

Users at the RCI can monitor the performance of the ADAPTS algorithm by looking at a graphical display of active beam positions (Fig. 2). Beam positions are color coded as follows: white beam positions are inactive, and green and yellow beam positions are active. Green beam positions meet the first and second detection criteria, whereas yellow beam positions correspond to the neighbor footprint extension (third criterion). The display updates every second and highlights in red the "current" beam position.

5. High-temporal sampling with the NWRT PAR

One of the key advantages of the NWRT PAR is the capability to produce the higher-temporal-resolution data desired by National Weather Service (NWS) forecasters (e.g., Steadham 2008), broadcast meteorologists in the southern plains (LaDue et al. 2010), and several government agencies (OFCM 2006, 9–21). Multipanel designs typical of PAR systems reduce the sampling time by having each panel scan only part of a 360° sector (Brookner 1988). This type of design is demonstrated by the 90° sector scanned by the NWRT PAR. As discussed in section 3, though, depending on the situation, update time can be traded for spatial resolution and/or data quality. This section uses case examples to illustrate some of the sampling techniques employed by the NWRT PAR for high temporal sampling of storms.

a. Achieving denser spatial sampling

When NEXRAD VCPs are employed by the NWRT PAR, temporal resolution is improved by a factor of 4 due to the smaller sector size: 90° versus 360°. Sampling storms with VCPs 11 and 12, for example, results in updates of 1.25 and 1.0 min, respectively. Given this significant improvement in temporal sampling, a relevant research question is: in what situations might it be worthwhile to slightly reduce the temporal sampling rate to improve the observations of storm structures?

1) DENSER VERTICAL SAMPLING

To study the advantages of dense vertical sampling, a scanning strategy with 25 tilts, spaced to provide a vertical overlap of up to one-half beamwidth, was developed and implemented in spring 2009. Rather than designing a "one size fits all" scanning strategy, two versions were
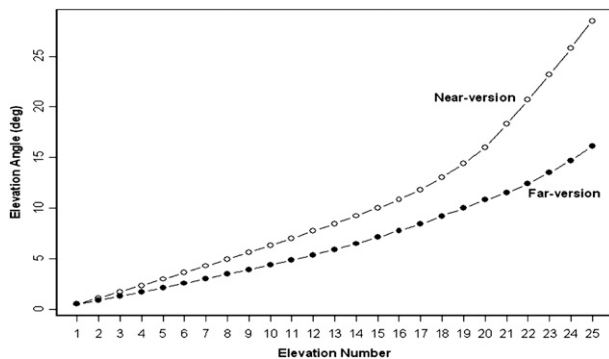
FIG. 3. The 25 elevation angles that define the near (open circles) and far versions (filled circles) of the dense vertical scanning strategy.

developed to better sample the vertical structure of storms located near and far from the radar (Fig. 3). The near version extended to 28.5° to provide sampling through higher heights close to the radar than typical scanning strategies. In contrast, the far version (radar range ≥ 80 km) extended to only 16.1° to avoid scanning above storm top height (assumed ≤ 18 km AGL), while providing even denser vertical sampling than the near scan (Fig. 3). In both versions the number of samples either matched or exceeded those of VCP 12 (NOAA 2006), and the PRTs were chosen to match the maximum expected range of storms. Slight adjustments to the PRTs and numbers of samples achieved the same update time for both versions. Data were collected using a batch PRT waveform and 1° azimuthal oversampling. This combination of scanning strategy characteristics produced an update time of ~2 min.

One radar-derived application that could benefit from dense vertical sampling is storm-top height estimates. Similar to the echo tops product from the WSR-88D, in this study storm-top height is defined as the highest height at which an 18-dBZ or higher reflectivity factor is sampled. Because uncertainty in storm-top height estimates is related primarily to the spacing between consecutive tilts, closer spacing reduces uncertainty. The impacts of dense vertical sampling on storm top estimates are illustrated in Fig. 4. In this case, a group of longitudinally oriented storms, located about 100 km from the NWRT PAR, were sampled at ~0352 UTC 13 May 2009 using the far version of the dense vertical scanning strategy (Fig. 3). Typically, the upper levels of storms (in this case 11–15 km MSL) located 100 km from the radar would be sampled by two elevation angles (2° increment) rather than by four (Fig. 4). If these two elevation angles were 6.48° and 8.46°, storm-top height estimates would be 14.9 km MSL for storm A and 11.8 km MSL for storms B–E. The dense vertical sampling better captures variations in storm-top height among

storms A–E (Fig. 4) and reduces the uncertainty of the estimates. The storm-top heights resulting from denser vertical sampling are A, 14.9 km; B, 13 km; C, 14 km; D, 12.6 km; and E, 11.8 km MSL. As mentioned earlier, the trade-off for dense vertical sampling is longer sampling time (2 versus 1 min).

Though the accuracy of several other radar-derived quantities may benefit from dense vertical sampling (e.g., vertical extent of circulations and high reflectivity cores or vertically integrated quantities), a more complete examination of them is beyond the scope of this paper.

2) DENSER AZIMUTHAL SAMPLING

The depiction of velocity signatures with significant gradients in the azimuthal direction depends strongly on azimuthal sampling. Similar to super-resolution sampling (Brown et al. 2002), 50% overlapped azimuthal sampling (0.75°–1.05°) was employed to improve the apparent resolution of azimuthal signatures sampled by the NWRT PAR. Because the beamwidth varies across the sector, the oversampling is adjusted accordingly. In this case, the increased number of azimuthal beam positions (55 without oversampling; 109 with 50% oversampling) at all elevations (14) increases the sampling time of the VCP. These sampling characteristics increased the volumetric sampling time from about 1 min to approximately 1.4 min.

A key velocity signature that can benefit from high-resolution azimuthal sampling is the mesocyclone signature. At 0131:24 UTC 1 May 2009, the NWRT PAR sampled the center of a mesocyclone signature located ~170 km west-northwest of the NWRT PAR (Fig. 5). At this location the azimuthal sampling spacing without oversampling was ~4.63 km, whereas with 50% oversampling the azimuthal sampling spacing was ~2.31 km. To simulate velocity and reflectivity fields without azimuthal oversampling, every other radial was removed from the oversampled data and then plotted for comparison. The comparison of the structure of the mesocyclone signature in the velocity field, and the structure of the inflow notch and hook echo in the reflectivity field, shows that these structures are more poorly resolved when azimuthal oversampling is not employed (Fig. 5).

b. Achieving further improvements to the temporal sampling via electronic scanning

The improved vertical and azimuthal spatial resolutions illustrated in Figs. 4 and 5 came at the expense of slightly slower update times. The remaining subsections describe three scanning methods that are either only feasible on, or are best suited for, electronically steered antennas. These methods can achieve the high-temporal-resolution sampling needed to observe rapid evolution in severe storms.
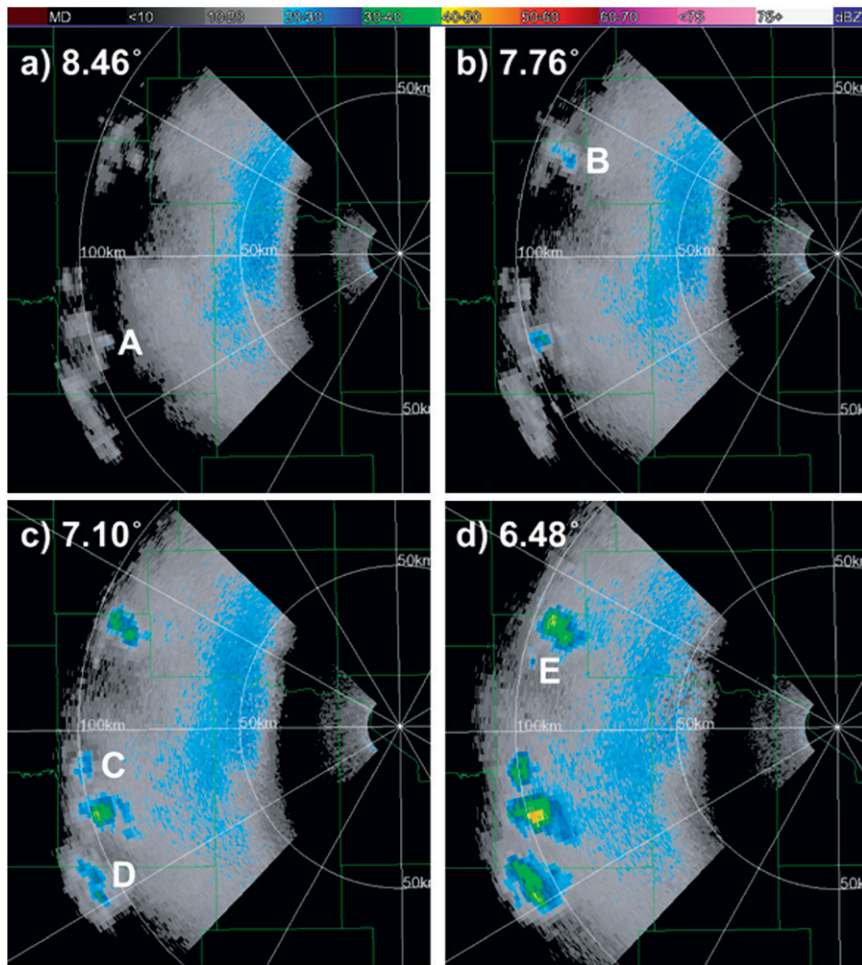
FIG. 4. Storm-top heights (18-dBZ echo) depicted by dense vertical sampling at ~0352 UTC 13 May 2009. Elevation angles are (a) 8.46°, (b) 7.76°, (c) 7.10°, and (d) 6.48°. Letters denote the tilt at which storm-top height was computed for each storm. Range rings are shown in 50-km increments.

1) BMX and sector scanning

On 19 August 2007, low-top supercells developed in a tropical environment rarely experienced in Oklahoma, a few hours prior to the reintensification of Tropical Cyclone Erin (Arndt et al. 2009). Due to the potential for tornado development, both high-temporal-resolution sampling (<1 min) and accurate estimates of radial velocity were desired. This goal was accomplished by implementing a BMX scanning strategy with the same 14 tilts as the NEXRAD VCP 12 (NOAA 2006). Accurate velocity and reflectivity estimates were obtained by sampling the storm with 64 pulses at all elevations. Velocity aliasing and update time were minimized by employing a uniform and lowest available PRT (0.8 ms). In this case, the uniform PRT was appropriate due to the lack of storm development beyond 120 km. The

azimuthal sampling spacing of velocity estimates was improved by fixed 0.5° oversampling. Without BMX, these scanning strategy characteristics would typically produce 132-s volumetric updates over a 90° sector. The implementation of BMX increased the temporal resolution by approximately a factor of 2, resulting in 63-s updates. In the example shown, the update time was reduced further, from 63 to 43 s, by manually decreasing the sector size to 60° (Fig. 6). The smaller sector size focused data collection on a low-top supercell located ~60 km from the NWRT PAR (Fig. 6a). At this radar range, the height of the 0.5° tilt was 0.8 km MSL and the spatial distance between azimuthal observations was 0.52 km.

The 43-s volumetric sampling captured the development of a cyclonic velocity couplet at the 0.5° elevation during 0141:27–0143:36 UTC 19 August 2007 (Fig. 6b).
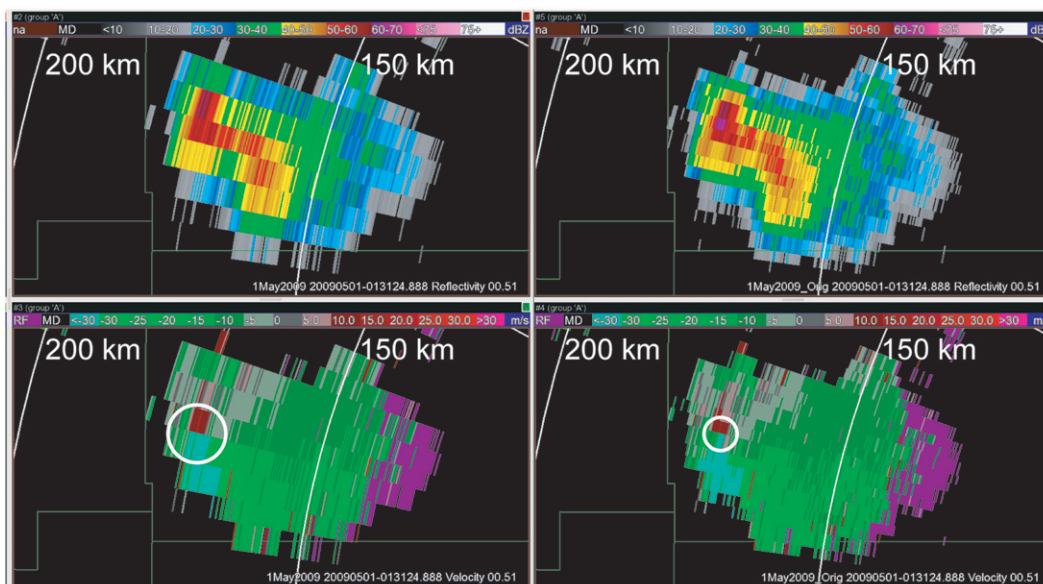
FIG. 5. Comparison of (top) reflectivity (dBZ) and (bottom) velocity (m s^{-1}) fields at 0.5° elevation with (left) 0% and (right) 50% azimuthal oversampling. The white circle denotes the mesocyclone circulation.

A damage survey later revealed that about 2 min after the velocity couplet first appeared on the NWRT PAR (Fig. 6c), a short-lived (~2 min) tornado occurred that produced category-1 damage on the enhanced Fujita (EF) scale along a swath 2.0 km long and 0.036 km wide (information online at http://ewp.nssl.noaa.gov/projects/shave/tornsurveys.php#map). During the tornado's short lifetime, the maximum measured gate-to-gate azimuthal velocity difference was 48 m s^{-1}. The rapid development and short-lived nature of this tornado illustrates the need for high-temporal-resolution data to sample this type of event. As mentioned previously, a drawback of this scanning strategy is that ground clutter filtering is currently unavailable for BMX. However, this was not an issue in this particular case because the storm of interest was located beyond the typical clutter field for the NWRT PAR.

2) ELEVATION-PRIORITIZED SCANNING

Elevation-prioritized scanning is designed to provide the fastest update rate at low-elevation angles and the slowest update rate at high-elevation angles. In this case, 14 tilts are elevation prioritized to accomplish the following within about 4 min (Fig. 7):

- six updates at the lowest two elevations,
- three updates at the next five elevations, and
- two updates at the highest six elevations.

Because of the interlaced nature of this scanning strategy, the temporal sampling rate at a fixed elevation angle varies. The time intervals between 0.5°-elevation scans, for example, range from 41 to 51 s, with a median time interval of 43.5 s. The median update times for the elevation-prioritized scanning strategy are as follows: the lowest two elevation angles, 43.5 s (0.73 min); the middle elevation angles, 87 s (1.45 min); and the upper-elevation angles, 132.5 s (2.2 min).

Like the dense vertical scanning strategy, the elevation-prioritized scanning strategy has two versions: near and far. Only the near version is described in detail (Fig. 7) because the storm in the case example was located within 50 km of the NWRT PAR. Both versions, however, operate similarly with the main difference being the specific elevation angles and PRTs employed.

The update times result from the number and temporal ordering of the elevation angles, the PRTs, azimuthal sampling, and number of pulses. To improve azimuthal sampling, the elevation-prioritized scanning strategy implements 50% overlapped azimuthal sampling at all elevation angles. To further improve detection of tornadic vortex signatures and other hazardous weather signatures, variance of velocity estimates at the lowest two tilts is minimized by collecting a relatively large number of pulses (64). The accuracy of the reflectivity data is also enhanced by collecting more than the traditional number of pulses (16) for all surveillance scans. The higher number of pulses provides less noisy depictions of hook echoes, bounded weak echo regions, and other reflectivity signatures associated with potentially severe convective storms.

On the evening of 13 May 2009 (CDT), a cyclic supercell moved across Oklahoma City, Oklahoma. Because tornado occurrence was a concern, high-temporal-resolution
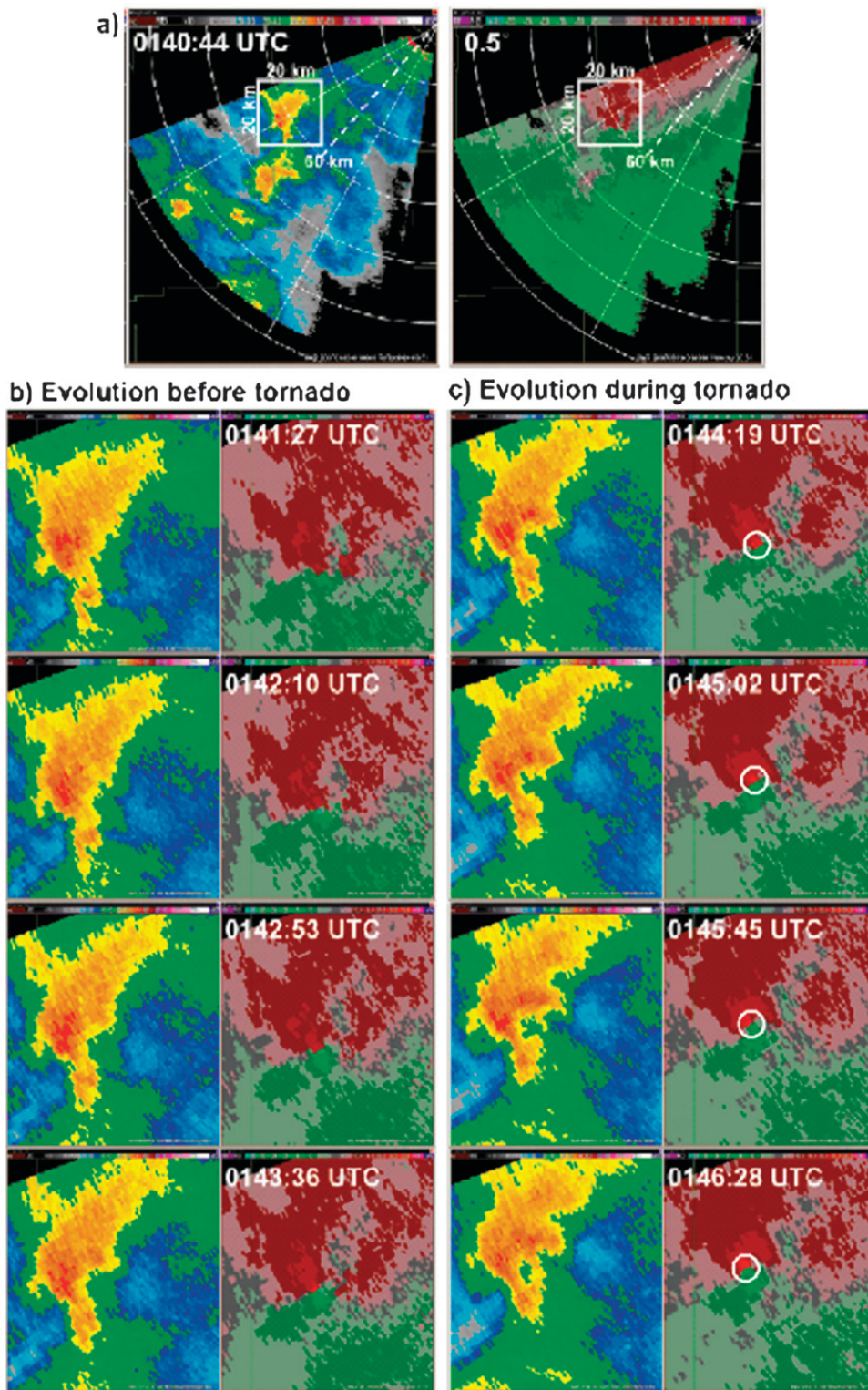
FIG. 6. (a) A 60° sector scan of 0.5°-elevation (left) reflectivity (dBZ) and (right) velocity (m s^{-1}) fields at 0140:44 UTC 19 Aug 2007. Range rings are in 20-km increments. The white box denotes the location and scale of the storm whose evolution at the 0.5° tilt is shown (b) prior to and (c) during an EF1-rated tornado. The white circles enclose the tornadic vortex signature.
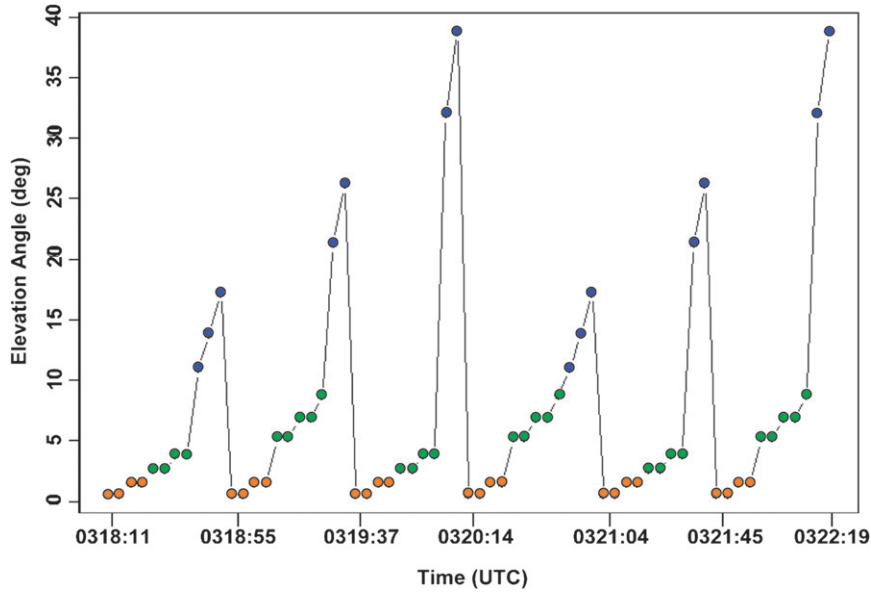
FIG. 7. Temporal order of elevation angles in the near version of the elevation-prioritized scanning strategy. The median temporal resolution is indicated by the colored dots: orange, 43.5 s (0.73 min); green, 87 s (1.45 min); and blue, 132.5 s (2.2 min).

sampling, especially at the lower elevations, was desired. As noted earlier, due to the storm's proximity to the NWRT PAR, the supercell was sampled with the near version of the elevation-prioritized scanning strategy (Fig. 7), which provided 43.5-s median updates at the two lowest elevations: 0.5° and 1.5°. These data were collected while the supercell's hook echo and several

mesocyclone circulations were located within 10–20 km of the NWRT PAR during 0318:11–0348:26 UTC 14 May 2009.

At 0339:25 UTC, a prominent cyclonic circulation at 0.5° elevation was sampled with a 0.22-km azimuthal spacing at a height of 0.5 km MSL (Fig. 8). To track the intensity of the initial and subsequent circulations, the
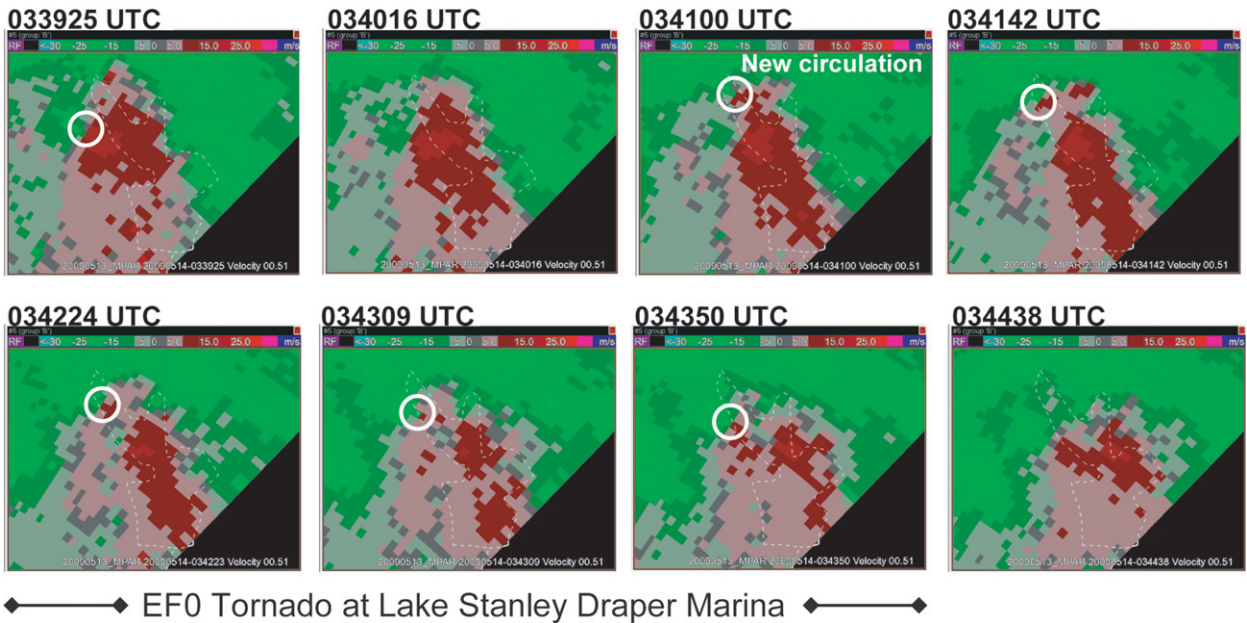

FIG. 8. A time series of NWRT PAR 0.5°-elevation radial velocity data prior to and during the EF0 tornado over Lake Stanley Draper. The white circles highlight the two significant cyclonic circulations discussed in the text.
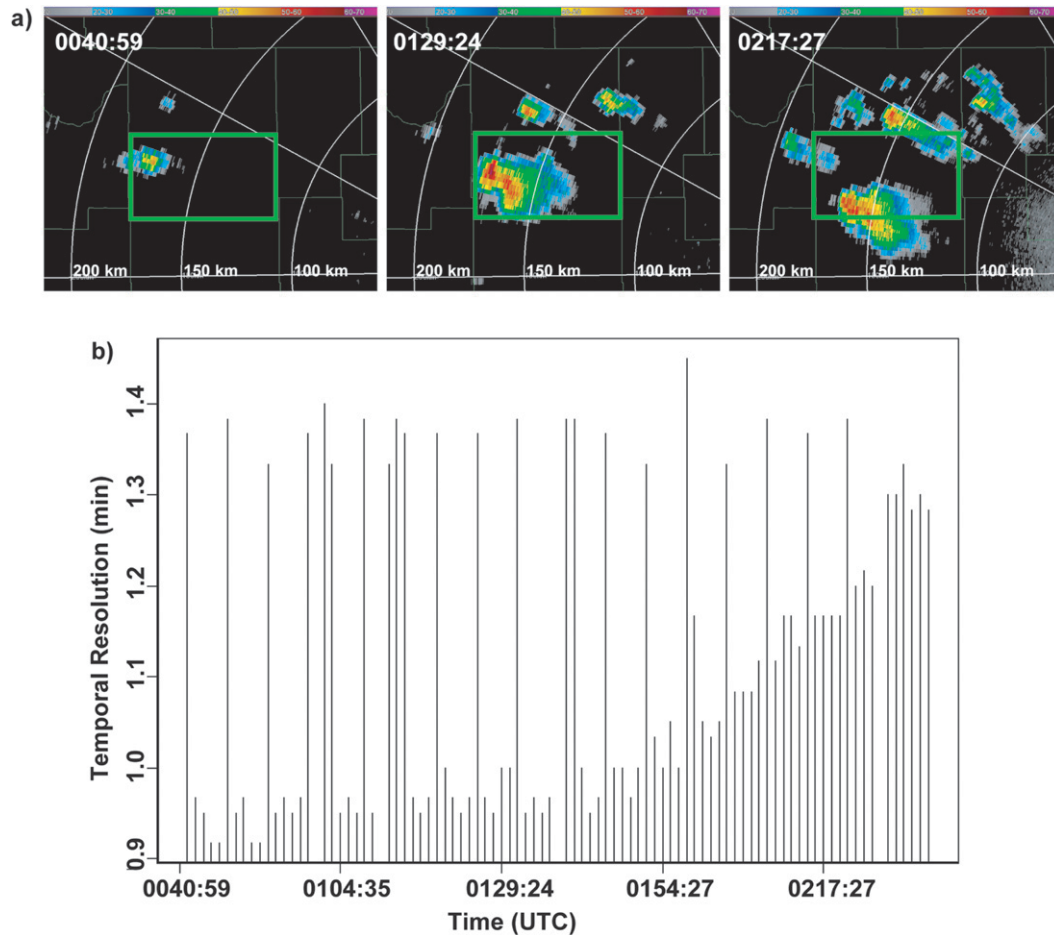
FIG. 9. (a) Three 0.5°-elevation reflectivity images illustrating the evolution of areal storm coverage on 1 May 2009. The green box outlines Custer County in west-central Oklahoma. (b) Time series showing temporal resolution of 102 volume scans collected within 0040:59–0244:03 UTC 1 May 2009. Blank areas within the time series indicate a break in data collection.

maximum azimuthal velocity difference within 1 km of the circulations' center was computed. Though the velocity difference associated with this first circulation was 23.5 m s^{-1} at 0339:25 UTC, it rapidly dissipated within the following 2 min. Within this same time interval, a new circulation developed ~1 km to the north of the former one (0341:00 UTC; Fig. 8). The initial velocity difference of this second cyclonic circulation was 26 m s^{-1} (0341:00 UTC); this intensity was maintained or exceeded during the next 5 min.

A comparison of the locations of this velocity signature with a damage survey (completed by the first author and L. Lemon, who is affiliated with the National Weather Service's Warning Decision Training Branch) concluded that a short-lived tornado producing EF0 damage occurred during the 0342:24 and 0343:50 UTC volume scans (Fig. 8). During its short duration, the maximum measured velocity difference

was 31.5 m s^{-1} (0.5 km MSL) at 0343:50 UTC. Within the tornado's lifetime, it crossed the marina on the western shore of Lake Stanley Draper and proceeded southward across a picnic area, parking lot, and walking path just east of a small pond, producing an approximate 0.80-km-long damage path. Once again, the rapid development and short-lived nature of this tornadic event illustrates the need for high-temporal-resolution radar data to detect the occurrence of similar types of events.

3) ADAPTIVE SCANNING

During 0040:59–0044:03 UTC 1 May 2009, data were collected on an isolated storm located in Custer County, Oklahoma (Fig. 9a). The storm developed into a nontornadic supercell that, according to a preliminary *Storm Data* report, produced up to baseball-sized hailstones

(2.75 in) at approximately 0200 UTC near Stafford, Oklahoma, in south-central Custer County (information online at http://www.spc.noaa.gov).

Because the storm was isolated, it was a good candidate for demonstrating and evaluating the potential utility of ADAPTS. As described in section 4, a primary goal of ADAPTS is to reduce scan time by sampling only regions containing weather features of interest, while capturing the growth, decay, and horizontal advection of existing storms. When ADAPTS is running, full volume scans are collected at ~5-min intervals, with adaptive scanning occurring between them.

Because of the storm's distance from the PAR (150–200 km) and a desire for rapid updates at all tilts, the storm was sampled with a far version of a conventional 14-tilt scanning strategy that extended to 15.5°. Like several of the other scanning strategies, this one employed 50% overlapped azimuthal sampling at all elevations; the PRTs ranged from 0.8 to 3.104 ms. These sampling characteristics resulted in approximately 1.4-min updates.

Figure 9b shows the improvement in temporal resolution attained from ADAPTS. The occasional gaps in the time series indicate loss of data collection owing to forced reboots of the RCI. The highest improvement in temporal resolution (0.9 min) occurs early in the storm's lifetime: 0040:59–0052:44 UTC. Over the next hour, volume updates of 1 min or less are maintained between volume scans (Fig. 9b). Thereafter, Fig. 9b shows a nearly linear increase in sampling time between 5-min intervals, which directly corresponds to an increase in the number of active beam positions. The contributing factors to the increase in active beam positions were an increase in the number of storms sampled and the horizontal (Fig. 9a) and vertical (not shown) storm growth as the storms advanced toward the NWRT PAR.

6. Conclusions

Under the umbrella of the multifunction phased-array radar (MPAR) initiative, scientists at the National Severe Storms Laboratory have been demonstrating unique PAR capabilities for weather observations in a multifunction environment. The focus of this work was the capability to observe weather phenomena with high temporal resolution. In addition to describing the engineering and software upgrades required to develop advanced scanning strategies for weather observations, we discussed the trade-offs that exist when designing scanning strategies that attempt to balance the need for faster updates with requirements for coverage and data quality. We presented examples of scanning strategies that trade update time for coverage and/or data quality and illustrated each of these with case data. The examples show that having phenomenon-based, adaptive scanning strategies is essential to fully capitalize on the benefits of PAR technology.

Although a comprehensive study of the improvements resulting from high temporal sampling of weather phenomena was beyond the scope of this study, it was demonstrated that PAR technology can be exploited to achieve results that are unfeasible with current operational technology. Nonetheless, more research is needed to translate these improvements into concrete, measurable, and meaningful service improvements for the National Weather Service. As such, researchers working with the NWRT PAR will continue to explore and demonstrate new capabilities to address twenty-first-century weather forecasting and warning needs.

REFERENCES

Arndt, D. S., J. B. Basara, R. A. McPherson, B. G. Illston, G. D. McManus, and D. B. Demko, 2009: Observations of the overland reintensification of Tropical Storm Erin (2007). *Bull. Amer. Meteor. Soc.,* **90,** 1079–1093.

Biggerstaff, M. I., and Coauthors, 2005: The Shared Mobile Atmospheric Research and Teaching Radar: A collaboration to enhance research and teaching. *Bull. Amer. Meteor. Soc.,* **86,** 1263–1274.

Bluestein, H. B., and R. M. Wakimoto, 2003: Mobile radar observations of severe convective storms. *Radar and Atmospheric Science: A Collection of Essays in Honor of David Atlas, Meteor. Monogr.,* No. 52, Amer. Meteor. Soc., 105–138.

——, M. M. French, I. PopStefanija, R. T. Bluth, and J. B. Knorr, 2010: A mobile, phased-array Doppler radar for the study of severe convective storms. *Bull. Amer. Meteor. Soc.,* **91,** 579–600.

Brookner, E., 1988: *Aspects of Modern Radar.* Artech House, 574 pp.

Brown, R. A., V. T. Wood, and D. Sirmans, 2002: Improved tornado detection using simulated and actual WSR-88D data with enhanced resolution. *J. Atmos. Oceanic Technol.,* **19,** 1759–1771.

Carbone, R. E., M. J. Carpenter, and C. D. Burghart, 1985: Doppler radar sampling limitations in convective storms. *J. Atmos. Oceanic Technol.,* **2,** 357–361.

Chrisman, J. N., 2009: Automated Volume Scan Evaluation and Termination (AVSET): A simple technique to achieve faster volume scan updates for the WSR-88D. Preprints, *34th Conf. on Radar Meteorology,* Williamsburg, VA, Amer. Meteor. Soc., P4.4. [Available online at http://ams.confex.com/ams/pdfpapers/155324.pdf.]

Doviak, R., and D. Zrnić, 2006: *Doppler Radar and Weather Observations.* 2nd ed. Academic Press, 562 pp.

Forsyth, D., and Coauthors, 2007: Update on the National Weather Radar Testbed (phased array). Preprints, *33rd Conf. on Radar Meteorology,* Cairns, QLD, Australia, Amer. Meteor. Soc., 7.4. [Available online at http://ams.confex.com/ams/pdfpapers/119631.pdf.]

Heinselman, P. L., D. L. Priegnitz, K. L. Manross, T. M. Smith, and R. W. Adams, 2008: Rapid sampling of severe storms by the National Weather Radar Testbed Phased Array Radar. *Wea. Forecasting,* **23,** 808–824.

——, and Coauthors, 2009: Phased array radar innovative sensing experiment. Preprints, *34th Conf. on Radar Meteorology,* Williamsburg, VA, Amer. Meteor. Soc., P6.5A. [Available online at http://ams.confex.com/ams/pdfpapers/155589.pdf.]

Jain, M., Z. Jing, A. Zahrai, A. Dodson, H. Burcham, D. Priegnitz, and S. Smith, 1997: Software architecture of the Nexrad open systems Radar Product Generator (RPG). Preprints, *13th Int. Conf. on Interactive Information and Processing Systems for Meteorology, Oceanography, and Hydrology,* Long Beach, CA, Amer. Meteor. Soc., 238–241.

Junyent, F., V. Chandrasekar, D. McLaughlin, E. Insanic, and N. Bharadwaj, 2010: The CASA Integrated Project 1 networked radar system. *J. Atmos. Oceanic Technol.,* **27,** 61–78.

Kumjian, M. R., A. V. Ryzhkov, V. M. Melnikov, and T. J. Schuur, 2010: Rapid-scan super-resolution observations of a cyclic supercell with a dual-polarization WSR-88D. *Mon. Wea. Rev.,* **138,** 3762–3786.

LaDue, D., P. Heinselman, and J. Newman, 2010: Strengths and limitations of current radar systems for two stakeholder groups in the southern plains. *Bull. Amer. Meteor. Soc.,* **91,** 899–910.

Lin, Y. J., T. C. Wang, and J. H. Lin, 1986: Pressure and temperature perturbations within a squall-line thunderstorm derived from SESAME dual-Doppler data. *J. Atmos. Sci.,* **43,** 2302–2327.

McLaughlin, D., and Coauthors, 2009: Short-wavelength technology and the potential for distributed networks of small radar systems. *Bull. Amer. Meteor. Soc.,* **90,** 1797–1817.

Miller, L. J., and R. A. Kropfli, 1980: The Multiple Radar Workshop, November 1979, Part II: Experimental design and processes. *Bull. Amer. Meteor. Soc.,* **61,** 1173–1177.

National Academies, 2008: *Evaluation of the Multifunction Phased Array Radar Planning Process.* National Academy Press, 79 pp.

NOAA, 2006: Doppler radar meteorological observations. Part C: WSR-88D Products and Algorithms, Federal Meteorological Handbook, FCH-H11C-2006, Office of the Federal Coordinator for Meteorological Services and Supporting Research, Rockville, MD. [Available online at http://www.ofcm.gov/fmh11/fmh11C.htm.]

OFCM, 2006: Federal research and development needs and priorities for phased array radar. FMC-R25-2006, Interdepartmental Committee for Meteorological Services and Supporting Research, Committee for Cooperative Research Joint Action Group for Phased Array Radar Project. [Available online at http://www.ofcm.gov/r25-mpar/pdf/00-opening.pdf.]

Priegnitz, D., P. Heinselman, S. Torres, and R. Adams, 2009: Improvements to the National Weather Radar Testbed radar control interface. Preprints, *34th Conf. on Radar Meteorology,* Williamsburg, VA, Amer. Meteor. Soc., P10.10. [Available online at http://ams.confex.com/ams/pdfpapers/155633.pdf.]

Qiu, C.-J., and Q. Xu, 1996: Least squares retrieval of microburst winds from single-Doppler radar data. *Mon. Wea. Rev.,* **124,** 1132–1144.

Steadham, R., 2008: *Volume Coverage Pattern Usage. Part 1, 2008 National Weather Service Field Study,* Radar Operations Center, Norman, OK, 28 pp. [Available from WSR-88D Radar Operations Center, 1200 Westheimer Dr., Norman, OK 73069.]

Torres, S., and D. Zrnić, 2003: Whitening in range to improve weather radar spectral moment estimates. Part I: Formulation and simulation. *J. Atmos. Oceanic Technol.,* **20,** 1433–1448.

——, and C. Curtis, 2007: Initial implementation of super-resolution data on the NEXRAD network. Preprints, *23rd Int. Conf. on Interactive Information and Processing Systems (IIPS) for Meteorology, Oceanography, and Hydrology,* San Antonio, TX, Amer. Meteor. Soc., 5B.10. [Available online at http://ams.confex.com/ams/pdfpapers/116240.pdf.]

——, Y. Dubel, and D. Zrnić, 2004: Design, implementation, and demonstration of a staggered PRT algorithm for the WSR-88D. *J. Atmos. Oceanic Technol.,* **21,** 1389–1399.

Vasiloff, S. V., R. J. Doviak, and M. T. Istok, 1987: Weather radar interlaced scanning strategy. *J. Atmos. Oceanic Technol.,* **4,** 245–249.

Warde, D., and S. Torres, 2009: Automatic detection and removal of ground clutter contamination on weather radars. Preprints, *34th Conf. on Radar Meteorology,* Williamsburg, VA, Amer. Meteor. Soc., P10.11. [Available online at http://ams.confex.com/ams/pdfpapers/155681.pdf.]

Weber, M. E., J. Y. N. Cho, J. S. Herd, J. M. Flavin, W. E. Benner, and G. S. Torok, 2007: The next-generation multimission U.S. surveillance radar network. *Bull. Amer. Meteor. Soc.,* **88,** 1739–1751.

Wilson, J. W., R. D. Roberts, C. Kessinger, and J. McCarthy, 1984: Microburst wind structure and evaluation of Doppler radar for airport wind shear detection. *J. Climate Appl. Meteor.,* **23,** 898–915.

Wurman, J., 2002: The multiple-vortex structure of a tornado. *Wea. Forecasting,* **17,** 473–505.

Yu, T.-Y., M. B. Orescanin, C. D. Curtis, D. S. Zrnić, and D. E. Forsyth, 2007: Beam multiplexing using the phased-array weather radar. *J. Atmos. Oceanic Technol.,* **24,** 616–626.

Yussouf, N., and D. J. Stensrud, 2010: Impact of phased-array radar observations over a short assimilation period: Observing system simulation experiments using an ensemble Kalman filter. *Mon. Wea. Rev.,* **138,** 517–538.

Zhang, G., R. Doviak, C. Curtis, and Q. Cao, 2008: Multi-patterns to reduce sidelobe effects on the National Weather Radar Testbed. Preprints, *Symp. on Recent Development in Atmospheric Application of Radar and Lidar,* New Orleans, LA, Amer. Meteor. Soc., P1.12. [Available online at http://ams.confex.com/ams/pdfpapers/130792.pdf.]

Zrnić, D. S., and Coauthors, 2007: Agile beam phased array radar for weather observations. *Bull. Amer. Meteor. Soc.,* **88,** 1753–1766.